Nonlinear Dyn (2018) 93:119–132
https://doi.org/10.1007/s11071-017-3741-5

ORIGINAL PAPER

Externally excited purely nonlinear oscillators: insights into their response at different excitation frequencies

Ivana Kovacic · **Stefano Lenci**

Received: 29 April 2017 / Accepted: 7 August 2017 / Published online: 18 August 2017

Abstract This study is concerned with forced damped purely nonlinear oscillators and their behaviour at different excitation frequencies. First, their dynamics is considered numerically for the response determined in the vicinity of a backbone curve with the aim of detecting coexisting responses that have not been found analytically so far. Both the cases of low and high excitation amplitudes are investigated. Second, the angular excitation frequency is lowered significantly for different powers of nonlinearity, and the system's behaviour is examined qualitatively, which has not been considered previously related to a general class of purely nonlinear oscillators. It is illustrated that the response at a low-valued angular excitation frequency has a form of bursting oscillations, consisting of fast oscillations around a slow flow. Finally, approximate analytical solutions are presented for the slow and fast flow for a general class of purely nonlinear oscillators.

I. Kovacic (✉)
Centre of Excellence for Vibro-Acoustic Systems and Signal Processing, Faculty of Technical Sciences, University of Novi Sad, Novi Sad 21000, Serbia
e-mail: ivanakov@uns.ac.rs

S. Lenci
Department of Civil and Building Engineering and Architecture, Polytechnic University of Marche, 60131 Ancona, Italy
e-mail: lenci@univpm.it

Keywords Pure nonlinearity · Forced response · Bifurcations · Multistability · Basins of attraction · Fast flow · Slow flow · Hysteresis

1 Introduction

Purely nonlinear oscillators represent a distinctive class of nonlinear oscillators whose restoring force F_r does not have a linear term but contains only a monomial term that is a power function of the displacement x:

$$F_\mathrm{r} \propto \mathrm{sgn}\,(x)\,|x|^{\alpha}\,, \tag{1}$$

where α is any positive real number higher than unity. The sign and absolute value functions are used in this definition to assure that F_r is an odd function of the displacement for all the values of α defined. Alternatively, the restoring force can also be written down as:

$$F_\mathrm{r} \propto x\,|x|^{\alpha-1}\,. \tag{2}$$

The well-known example of this class of oscillators is a pure cubic one $\alpha = 3$, which can be obtained approximately by combining and tuning the parameters of several linear springs: two oblique ones with one vertical spring [1]. Besides being related to physical configurations [1,2], this type of a restoring force can also be related to purely nonlinear material properties [3]. Non-integer powers the force–displacement relationship have also been recognized in the suspension of the vehicle, micro-actuators and in the interaction

between the beads in the study of impulse propagation in a chain of elastic beads (see [4] and the references cited therein). Furthermore, power-law characteristics of the restoring force provide smooth approximations of non-smooth forces, as occurs for example in piecewise linear systems. The previous reasons provide a strong motivation for examining thoroughly their dynamic behaviour.

Undamped and damped unforced (free) responses of purely nonlinear one-degree-of-freedom oscillators have been widely examined by different techniques [5]. However, there has been a significantly smaller number of studies of harmonically excited purely nonlinear oscillators with an arbitrary positive power of nonlinearity. These studies can be divided into two groups: those concerned with pure cubic cases [6–8] and those covering a wider range of the power of nonlinearity [9–11]. To determine different types of their steady-state forced response, Hayashi [6] applied either the harmonic balance method or a perturbation technique in which an amplitude and a phase are expanded in terms of a small ordering parameter. For the application of the latter, he added a linear geometric term to both sides of the equation of motion. Burton [7] considered undamped harmonically excited pure cubic oscillators with an arbitrary magnitude of the ordering parameter. He utilized the Lindstedt–Poincaré method, but introduced a new expansion parameter, transforming a strongly nonlinear system to a weakly nonlinear system. He also showed that the approach with the square of the excitation frequency expanded in terms of the detuning yields the more accurate low order frequency–amplitude equation than the case when one uses a linear form of the forcing frequency in this relationship. Burton and Rahman [8] developed a multiple-scale technique for the damped harmonically excited system and also introduced a new expansion parameter, defined it as a deviation between the square of the excitation frequency and a backbone curve. In addition, they generalized their approach to the case of a nonlinear restoring force with any odd power of nonlinearity. In [9], a steady-state response in the vicinity of a backbone curve and the corresponding frequency–response curves are obtained for linearly viscously damped externally excited oscillators with weak and strong nonlinearity by using trigonometric functions. In [10], the extension to any power-form damping term is provided. Elliptic functions are utilized in [11] to deal with the existence of a general non-conservative term in the equation of motion and to improve the accuracy of the approximate solution.

The following study aims at extending considerations of the dynamics of harmonically excited viscously damped purely nonlinear oscillators governed by

$$\ddot{x} + 2\zeta\dot{x} + \varepsilon x|x|^{\alpha-1} = F\cos(\Omega t), \tag{3}$$

where the coefficient ε is positive, but not necessarily small. The goal is to provide further insights into their dynamical behaviour in two respects: first, to detect other coexisting responses that could not be found analytically in [9] for the same parameter values (Sect. 2), and second, to show how the system behaves when the angular excitation frequency is lowered significantly for different powers of nonlinearity (Sect. 3), which has not considered so far for a general class of purely nonlinear oscillators. These investigations contain both numerical and analytical considerations.

2 Overall dynamical behaviour

According to the results from [9], the frequency–response curves of the oscillators governed by Eq. (3) are given by

$$\Omega^2 = b_{1_\alpha}\varepsilon a^{\alpha-1} - 2\zeta^2 \mp \sqrt{\frac{F^2}{a^2} - 4\zeta^2 b_{1_\alpha}\varepsilon a^{\alpha-1} + 4\zeta^4}, \tag{4}$$

where a is the amplitude of the term that has the frequency Ω (note that the response obtained contains the third harmonic as well), while the constant b_{1_α} depends on the power of nonlinearity as follows:

$$b_{1_\alpha} = \frac{2}{\sqrt{\pi}}\frac{\Gamma\left(1+\frac{\alpha}{2}\right)}{\Gamma\left(\frac{3+\alpha}{2}\right)}, \tag{5}$$

with Γ being the Euler–Gamma function [12]. This approximate result, which is valid close to the backbone curve for ε that need not to be small, will be used to illustrate the frequency–response curves and to point out the frequencies at which additional numerical insights will be provided as a results of systematic numerical investigations for low and high excitation amplitude.

2.1 Numerical simulations

2.1.1 Low excitation amplitude

First, the following set of the system parameters is used: $\zeta = 0.025$, $\varepsilon = 0.1$ and $F = 0.1$. Note that these values correspond to the values used in Fig. 4 in [9]. The frequency–response curves are produced herein based on Eqs. (4) and (5) for different powers of nonlinearity to emphasize the important findings detected numerically, as explained below. So, Fig. 1 presented herein contains six frequency–response curves. To complement this presentation, the brute force bifurcation diagram is reported in Fig. 2

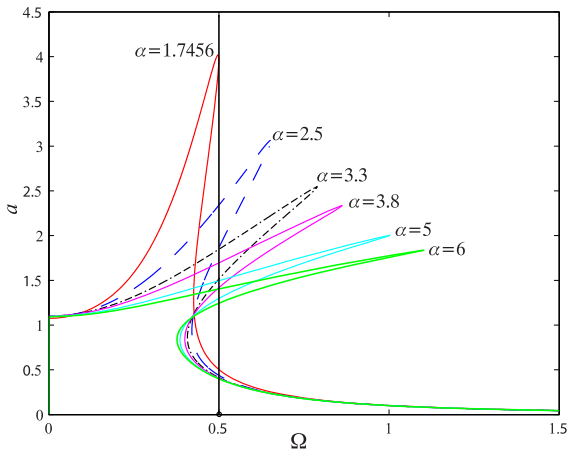

Fig. 1 Frequency–response *curves* defined by Eqs. (4) and (5) for $\alpha = 1$ and different powers of nonlinearity and for $\zeta = 0.025$, $\varepsilon = 0.1$ and $F = 0.1$

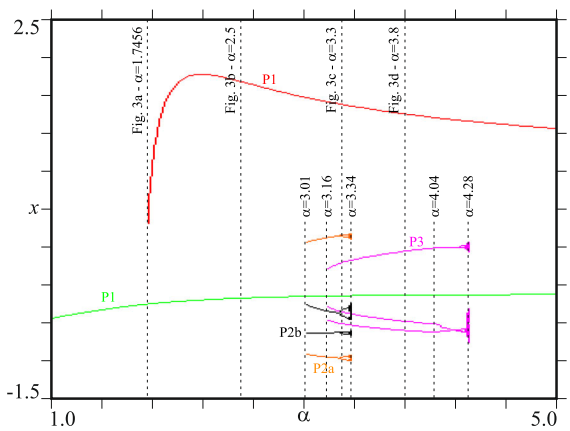

Fig. 2 Bifurcation diagram for increasing α and for $\zeta = 0.025$, $\varepsilon = 0.1$, $F = 0.1$ and $\Omega = 0.5$ (this value is also labelled in Fig. 1)

for $\Omega = 0.5$ (indicated in Fig. 1) for increasing α. To draw this picture (as well as forthcoming Fig. 5), the considered α interval is subdivided in 300 points. For each of these α-values, fourth-order Runge–Kutta numerical simulations (with 30 time steps per excitation period $T = 2\pi/\Omega$) are performed, and after a transient of 150 periods, the values of x at each period are reported. The intermediate branches (e.g. those of the minor attractors) are detected using an initial point taken from the relevant basin of attraction, for a value of α in between the range of existence of the attractor.

Five attractors can be seen: the most important is reported in green (colours are seen in the online version of the paper)—it is a non-resonant attractor that exists for all values of α. The resonant attractor is reported in red, and it is born by a Saddle-Node (SN) bifurcation at $\alpha \approx 1.745$. It always exists and is stable above this threshold in the considered range of α. It is also seen that the non-resonant attractor is a unique attractor below $\alpha \approx 1.745$.

There are also three minor attractors, which influence the global dynamics. The first two are two period-2 oscillations (reported in black and orange in Fig. 2), which are born by a SN bifurcation at $\alpha \cong 3.01$. They exist in a small interval, then undergo a classical Period-Doubling (PD) cascade ending with a Boundary Crises (BC) at $\alpha \approx 3.34$. They are symmetric with respect to each other. It should be pointed out that it is not so common to have period-2 oscillations born via a SN bifurcation, as period 2 oscillations usually come from PD bifurcations. Thus, this represents a characteristic of the system under consideration.

The third minor attractor, which is reported in magenta, has period 3. It is born by a SN bifurcation at $\alpha \approx 3.16$, undergoes a PitchFork (PF)—or symmetry breaking—bifurcation at $\alpha \approx 4.04$ (note that this is barely visible in Fig. 2), then a PD cascade follows ending with a final BC at $\alpha \approx 4.28$.

As another numerical insight, the basins of attractions just after the SN bifurcation appearance of the resonant attractor is reported in Fig. 3. Note that all of them correspond to the powers of nonlinearity used in Fig. 1. It is seen in Fig. 3a that for $\alpha \approx 1.7456$ the non-resonant (green) attractor is dominant. The basins boundaries are smooth.

For increasing α, the resonant (red) attractor becomes dominant (Fig. 3b), and the basins boundaries start to become wavy.

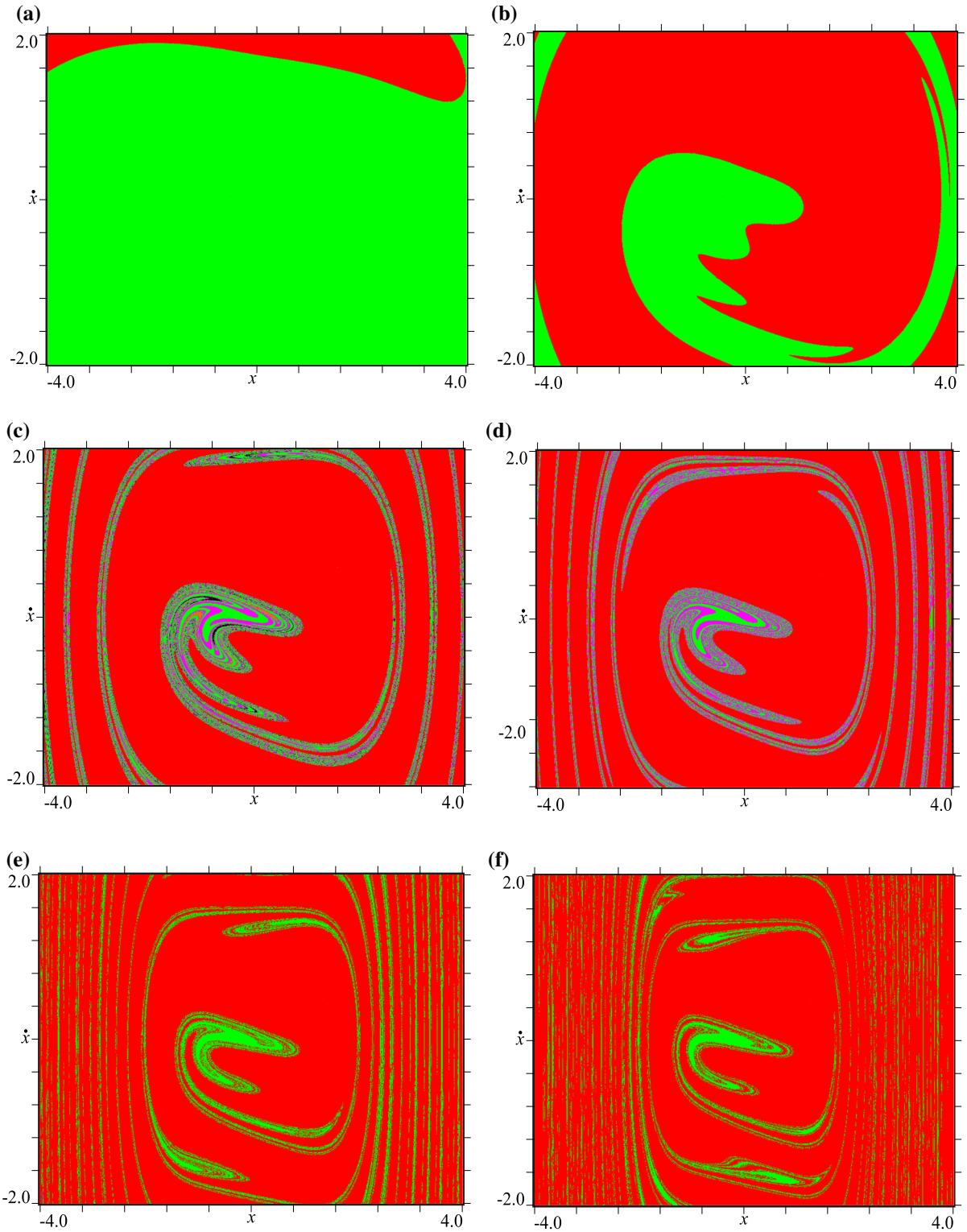

Fig. 3 Basins of attraction for $\zeta = 0.025$, $\varepsilon = 0.1$, $F = 0.1$, $\Omega = 0.5$ and **a** $\alpha = 1.7456$, **b** $\alpha = 2.5$, **c** $\alpha = 3.3$, **d** $\alpha = 3.8$, **e** $\alpha = 5$ and **f** $\alpha = 6$. The *colour* of the basin of each attractor is the same used for the corresponding path in Fig. 2. (Color figure online)

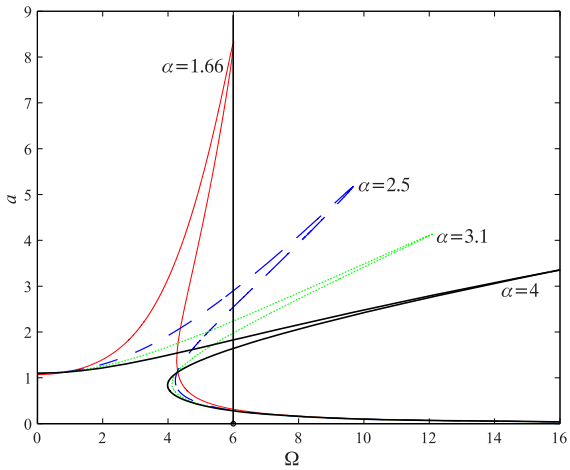

Fig. 4 Frequency–response *curves* defined by Eqs. (4) and (5) for different powers of nonlinearity and for $\zeta = 0.1$, $\varepsilon = 10$ and $F = 10$

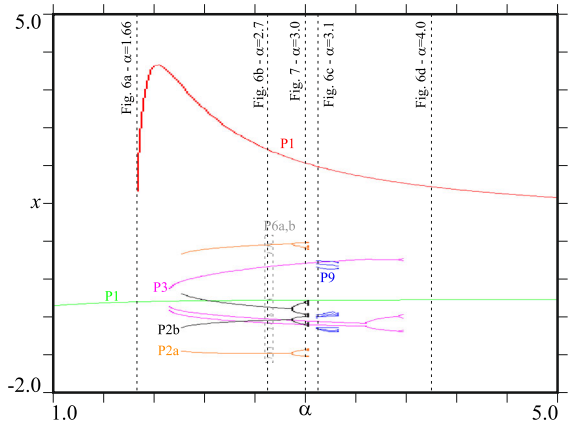

Fig. 5 Bifurcation diagram for increasing α and for $\zeta = 0.1$, $\varepsilon = 10$, $F = 10$ and $\Omega = 6$ (this value is also labelled in Fig. 4)

For $\alpha = 3.3$ (Fig. 3c), one can see five attractors that coexists in a very narrow domain. The boundaries of the red basins are still regular, while very oscillating. On the other hand, the boundaries of the basins of the non-resonant one and of the minor attractors (magenta, black and orange) are fractals, which affects the dynamical integrity [13,14] of these solutions.

The fractality of the basins of the small amplitude solutions survives after the disappearance of the period-2 solutions (Fig. 3d).

After the third minor attractor (magenta) disappearance, also the basin of a resonant attractor (red) becomes fractal (Fig. 3e), likely as a consequence of heteroclinic bifurcations occurred in the meanwhile. This situation persists up to very large values of α (Fig. 3f), where the fractality is very extended for large values of x.

2.1.2 High excitation amplitude

Second, as a representative of a high excitation amplitude case, the following set of the system parameters is used: $\zeta = 0.1$, $\varepsilon = 10$ and $F = 10$. These are the parameters also used in Fig. 5 of [9]. Herein, based on Eqs. (4), (5) and for different powers of nonlinearity, four frequency–response curves are plotted in Fig. 4. These frequency–response curves will be related to numerical results reported subsequently.

The bifurcation diagram is shown in Fig. 5 for increasing values of the power of nonlinearity α. There are the same five attractors already seen in Fig. 2 for a low excitation amplitude: a period-1 non-resonant one (green); period-1 resonant one (red); two symmetric period-2 ones (black and orange); period-3 (magenta). They have the same qualitative behaviour, in particular the sequence of bifurcations leading to their appearance/disappearance. However, they differ from a quantitative point of view. For example, the non-resonant attractor is born via a SN bifurcation at $\alpha \approx 1.66$.

There is a new, period-9 attractor, reported in blue in Fig. 5. It is born by a SN, undergoes a PF, then a PD cascade up to a BC, where it disappears. It exists in a very narrow range of the power of nonlinearity ($3.09 < \alpha < 3.26$), and thus it is a minor attractor. There are also two other very minor attractors, of period 6, reported in grey and light orange and in Fig. 5, symmetric between each other (see forthcoming Fig. 8f, g). They exists only in the neighbourhood of $\alpha = 2.7$.

The basins of attraction appearing just after the resonant attractor is born are reported in Fig. 6a. The resonant attractor has a very large amplitude (note that, to have the resonant attractor inside the considered window, the axes of Fig. 6a are larger than those of the others in Fig. 6), and initially its basin is small.

By increasing α, the red basin rapidly becomes dominant, as shown in Fig. 6b. It is also possible to see in this figure the existence of a main non-resonant attractor (green basin), and a minor period 3 (magenta basin) and period 2 (black and orange basins) attractors. They have fractal basin boundaries, with the fractal behaviour increasing for large oscillation amplitudes. The boundaries of the resonant attractor, on the other

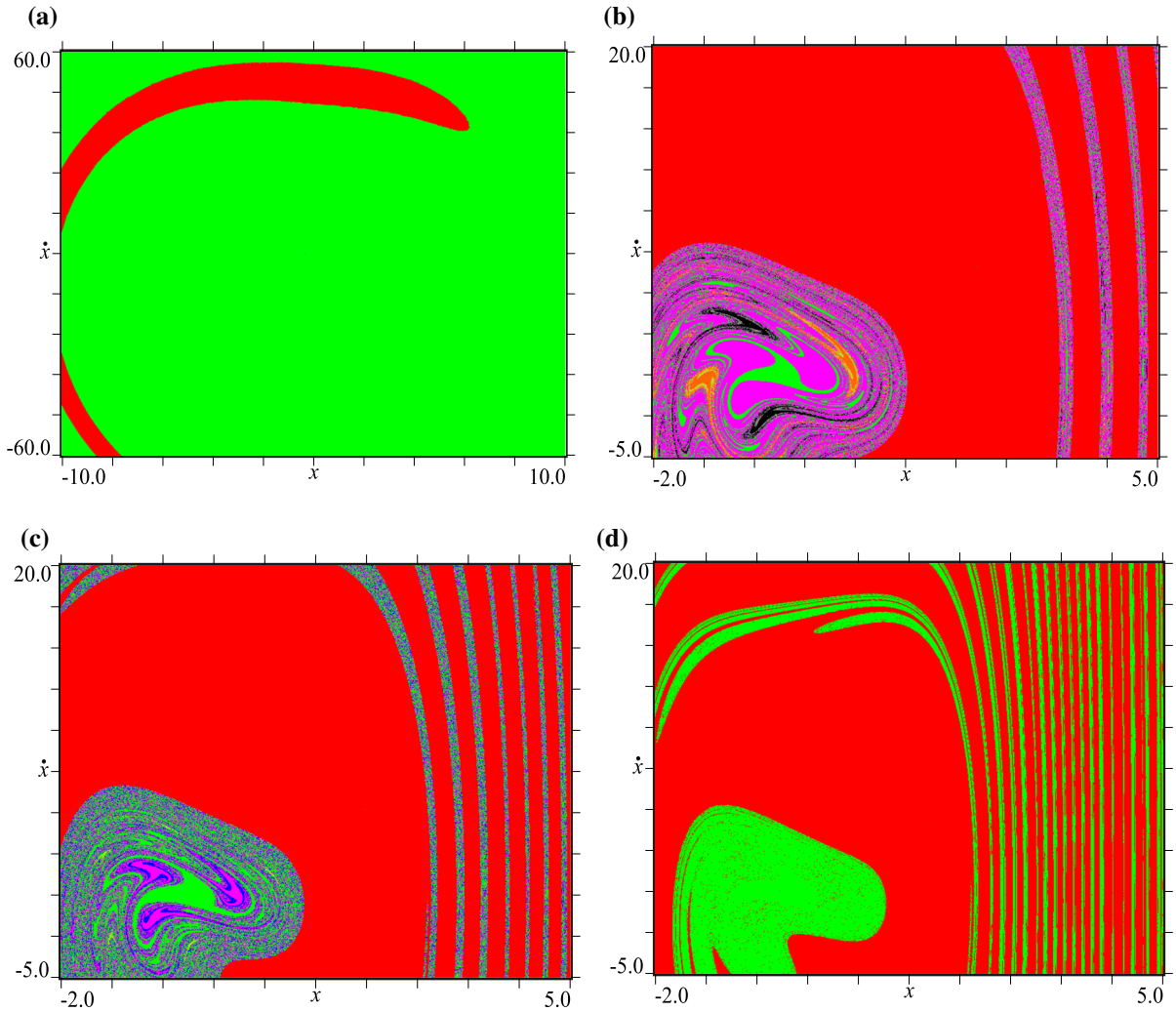

Fig. 6 Basins of attraction for $\zeta = 0.1$, $\varepsilon = 10$, $F = 10$, $\Omega = 6$ and **a** $\alpha = 1.66$, **b** $\alpha = 2.7$, **c** $\alpha = 3.1$ and **d** $\alpha = 4.0$. The *colour* of the basin of each attractor is the same used for the corresponding path in Fig. 5, as well as the same used in Fig. 7. (Color figure online)

hand, are smooth. There are also two very minor period 6 attractors (grey and light orange basins): their basins surround the basins of the period 2 attractors, and they are very small. Thus, these very minor attractors exist in an extremely narrow value of the parameters, and, what is more, they are difficult to be detected due to their very small basins in the existence range.

By further increasing α, one can observe four different coexisting attractors shown in Fig. 6c. Period 2 attractors have been substituted by a period 9 (blue basin) attractor yet seen in Fig. 5. The basins are even more fractal with respect to the previous case, entailing a further reduction of the dynamical integrity, i.e., the compact part of the basin of attraction around the corresponding attractor [13,14], and thus diminishing the robustness and then the practical usability of the bounded attractors.

Finally, when the period 9 disappears, only the resonant and non-resonant attractors remains, as seen in Fig. 6d. We note that the red tongues of the basin of the resonant attractor are entering the (green) basin of the non-resonant attractor, starting a fractalization that further develops by increasing α.

The main dynamical characteristic highlighted by the previous simulations is the occurrence of minor attractors.

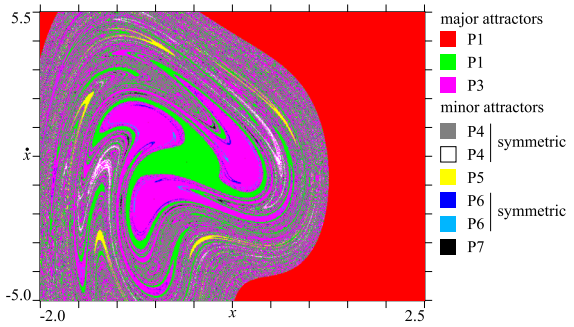

Fig. 7 Basins of attraction for $\zeta = 0.1$, $\varepsilon = 10$, $F = 10$, $\Omega = 6$ and $\alpha = 3.0$. (Color figure online)

It is worth highlighting that it is very difficult to detect these minor attractors, as one needs to build the basins of attraction just for a value of α belonging to their very narrow existence range.

Six minor attractors, coexisting with the three major attractors, are reported in Fig. 7. Two period 4 attractors appear after the PD of the period 2 attractors previously seen. In addition, there are: one period 5 attractor, two symmetric period 6 attractors and a period 7 attractor. Their phase portraits are reported in Fig. 8.

Since the minor attractors exist in a very narrow range (even smaller than that of P6 in Fig. 5), they are not reported in the bifurcation diagram of Fig. 5.

As expected, all periodic attractors with an even period exist with their symmetric counterparts, while this does not occur to odd-periodic attractors.

Figure 7 highlights another distinguished peculiarity of the considered system, namely the coexistence of many attractors (up to nine) of almost all periods (only period 2 is missing in Fig. 7).

Although we have not continued the research of minor attractors, we are quite sure that many other of them exists spread in the parameters space.

2.2 Analytical approximations of periodic solutions

In this section, we look for an analytical approximation of periodic solutions

$$x(t) = a\sin(\Omega t), \tag{6}$$

of the governing Eq. (3) rewriting it as

$$\ddot{x} + 2\zeta\dot{x} + \varepsilon x|x|^{\alpha-1} = F\sin(n\Omega t + \phi). \tag{7}$$

The integer n is introduced to consider period n oscillations, while the phase ϕ is due to damping. Inserting it in the excitation instead of in the solution is suitable to facilitate the following mathematical computations. For the same reasons, we consider the sine function instead of the cosine function.

The equations for the unknown a and ϕ are obtained by the Galerkin method. Multiplying Eq. (7) with $\sin(\Omega t)$, integrating it from $t = -\pi/\Omega$ to $t = \pi/\Omega$ and remembering that $x(t)$ is odd with respect to $t = 0$ and that $\sin(\Omega t)$ is always positive in $[0, \pi/\Omega]$, we obtain

$$-a\Omega^2 + \frac{2F\sin(\pi n)\cos(\phi)}{\pi(n^2-1)} + \varepsilon a^{\alpha} b_{1\alpha} = 0, \tag{8}$$

where $b_{1\alpha}$ is defined by Eq. (5).

Multiplying Eq. (7) with $\cos(\Omega t)$ and integrating it from $t = -\pi/\Omega$ to $t = \pi/\Omega$, one can derive

$$2a\zeta\Omega + \frac{2F\sin(\pi n)n\sin(\phi)}{\pi(n^2-1)} = 0. \tag{9}$$

For $n \neq 1$, Eqs. (8) and (9) are satisfied by $\zeta = 0$ and

$$a^{\frac{\alpha-1}{2}} = \Omega\sqrt{\frac{1}{\varepsilon b_{1\alpha}}}. \tag{10}$$

This provides the relation between the frequency and the amplitude of undamped free oscillations, and its geometric presentation gives a backbone curve. It is worth to note that for $\alpha < 1$, one has $a \to \infty$ for $\Omega \to 0$, so that the amplitude is inversely proportional to the frequency, while for $\alpha > 1$, one has $a \to 0$ for $\Omega \to 0$, and the amplitude in directly proportional to the frequency.

If $1 < \alpha < 3$, then $\frac{da}{d\alpha} \to 0$ for $\Omega \to 0$, so that for small values of Ω the vibration amplitude is infinitesimal, while for $\alpha > 3$ we have $\frac{da}{d\alpha} \to \infty$ for $\Omega \to 0$, namely even for very small Ωs the oscillation has a finite amplitude. For $\alpha = 3$ the relation between a and Ω is linear, this making the cubic case a special one.

Since F disappears, the proposed analytical approximation is not able to detect forced oscillations with $n \neq 1$.

When $n = 1$, Eqs. (8) and (9) simplify to

$$-\Omega^2 a - F\cos(\phi) + \varepsilon a^{\alpha} b_{1\alpha} = 0, \tag{11}$$

and

$$2\Omega a\zeta - F\sin(\phi) = 0. \tag{12}$$

Eliminating the phase angle ϕ from the previous equations, one derives

$$(2\Omega a\zeta)^2 + \left(\varepsilon a^{\alpha} b_{1\alpha} - \Omega^2 a\right)^2 = F^2, \tag{13}$$

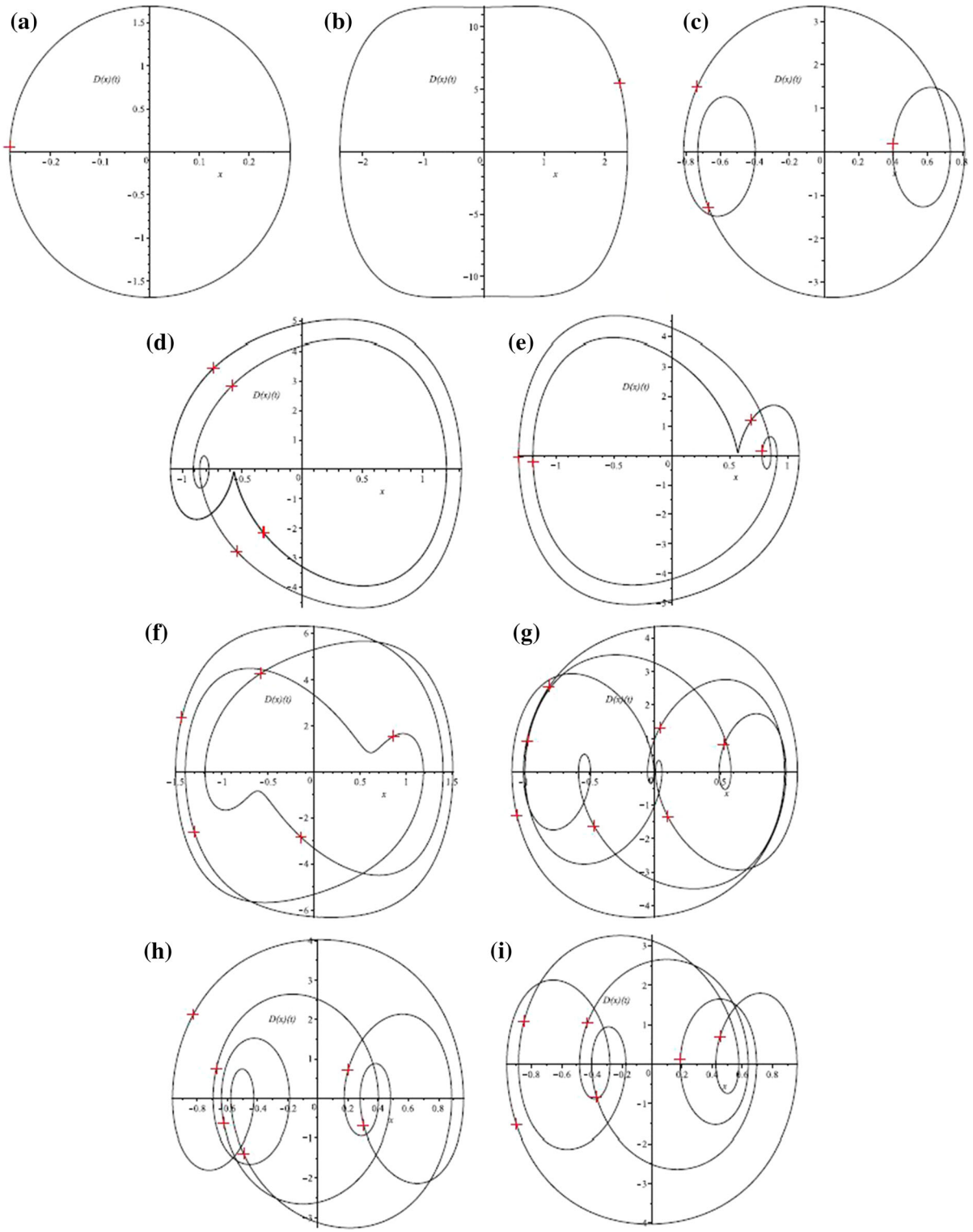

Fig. 8 Phase portraits of the nine attractors from Fig. 7. The *red* crosses are the points in the stroboscopic Poincarè map. **a** P1 non-resonant, **b** P1 resonant, **c** P3, **d** P4, **e** P4, **f** P5, **g** P7, **h** P6, **i** P6. The symmetry of the two period 4 and period 6 attractors is evident

which provides the amplitude of the oscillation a as a function of the system parameters ζ, ε and α and the excitation amplitude F and frequency Ω. When solved for Ω, this equations turns into Eq. (4). The fact that the same equation is obtained here with a different analytical technique confirms its reliability.

3 Dynamical behaviour at decreasing and low angular excitation frequency

3.1 Numerical insight

In order to give additional insights into the dynamic behaviour when Ω is decreased from the values used in Sect. 2.1.2, Fig. 9 is created showing the responses obtained numerically from Eq. (3) and superimposed onto the S-curve (nullcline):

$$\varepsilon x|x|^{\alpha-1} = F. \tag{14}$$

This curve is plotted as a red dashed line, while the response is plotted in black as changing with the excitation force $F\cos(\Omega t)$. The power of nonlinearity is fixed to $\alpha = 2.5$, while the excitation frequency is decreased, taking the values: $\Omega = 6, 4, 2, 0.6, 0.4, 0.2$. The shape of the response with respect to the lower and upper branch of the S-curve can be used to interpret the content of the responses, whose change in the character is shown for illustration in the time domain as well. When Ω is very small, as shown in Fig. 10a, b for $\alpha = 2.5$, $\Omega = 0.06$, the time response consists of the damped fast oscillations along the slow flow, which coincides with the branches of the S-curve (14). The hysteretic path followed by the time response is indicated by the arrows in Fig. 10a: starting from the left down part at Point A, the flow goes along the lower red branch of the S-curve, then jumps from the lower branch to the upper branch, passes through Point C on it and starts oscillating around the upper branch with a decreasing amplitude, then changes the direction at Point D, goes back along the upper branch, then jumps down, passes through Point B and oscillates around the lower branch until Point A. This hysteretic behaviour repeats afterwards periodically.

The way how the hysteretic behaviour looks like when imposed on the S-curve for the fixed low-valued excitation angular frequency and an increasing power of nonlinearity is shown in Fig. 11 for the $\alpha = 1.66$,

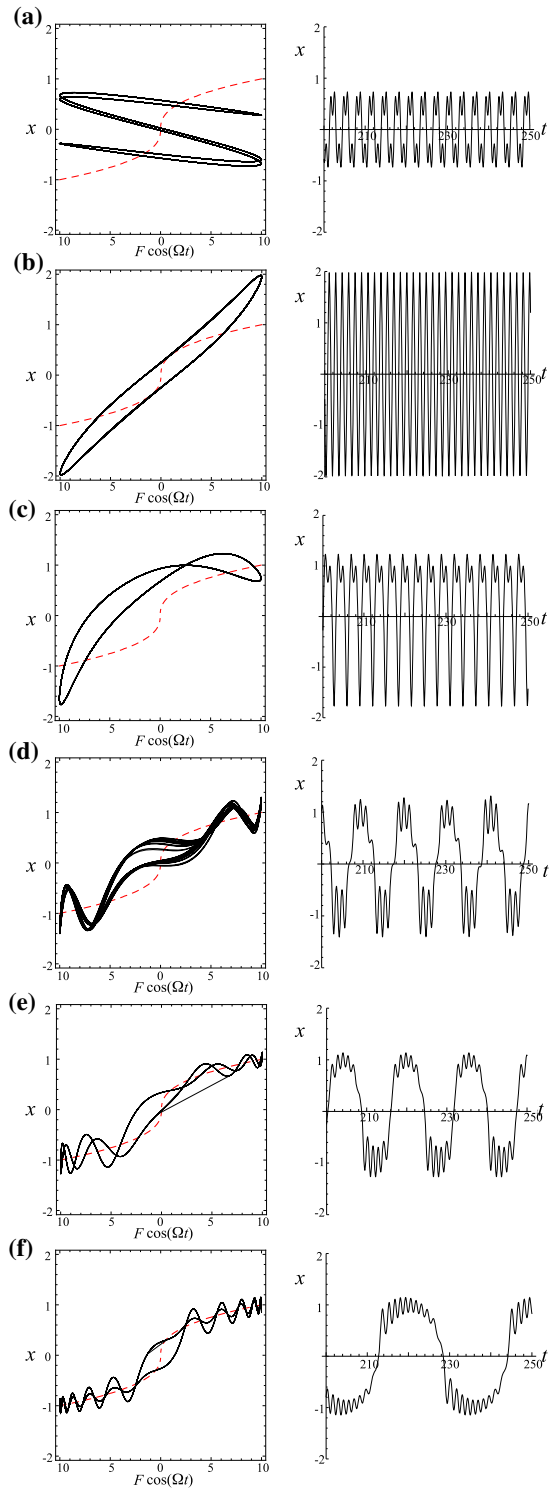

Fig. 9 Responses obtained numerically from Eq. (3) for $\zeta = 0.1$, $\varepsilon = 10$, $F = 10$, $\alpha = 2.5$ superimposed onto the *S-curve* (14) (*left*) and the corresponding time-histories plotted for: **a** $\Omega = 6$, **b** $\Omega = 4$, **c** $\Omega = 2$, **d** $\Omega = 0.6$, **e** $\Omega = 0.4$, **f** $\Omega = 0.2$

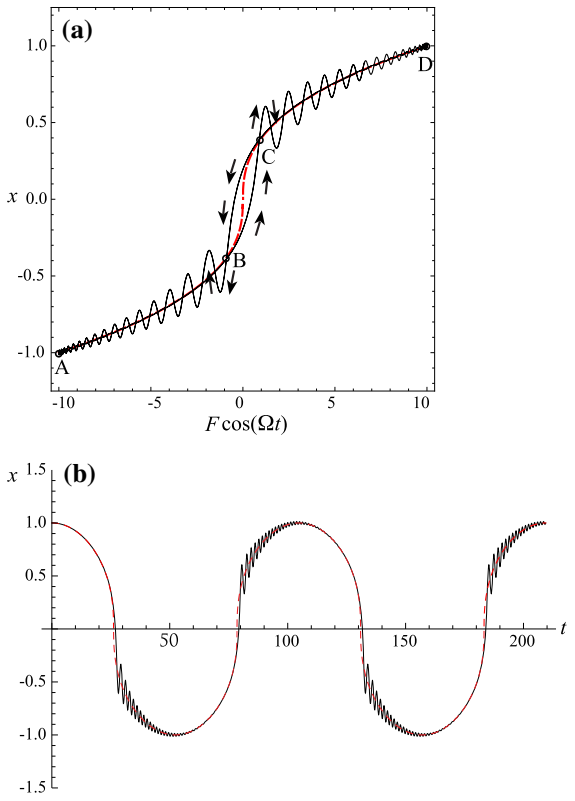

Fig. 10 **a** Response obtained numerically from Eq. (3) for $\zeta = 0.1$, $\varepsilon = 10$, $F = 10$, $\alpha = 2.5$, $\Omega = 0.06$ superimposed onto the *S-curve* (14) with some characteristic points of a hysteretic path labelled, **b** the corresponding time-histories and the slow flow (*red dashed line*) defined by Eqs. (18) and (19). (Color figure online)

3.1, 4, which are the parameters used in Fig. 6. The corresponding time responses are also presented.

A remark should be made here about the fact that the (fast dynamics) bursting oscillations are generated when the solution passes through $x = 0$, namely at the unique non-smooth point of the restoring force. Thus, its mechanical motivation is clear, and it is remarkable that this very weak non-smoothness (the force is continuous, and only its derivative of order $[\alpha] + 1$ is discontinuous) has so important dynamical effects.

3.2 Analytical approximations of bursting oscillations

In has been illustrated above that purely nonlinear oscillators subject to external excitation with low-valued angular frequency can exhibit a response that consists of fast flow oscillations around the periodical slow flow. The aim of the following analysis is to obtain approximate analytical expressions for these slow and fast flows and the overall response. So, the overall solution is represented as the sum of the slow flow x_s and the fast flow X_f,

$$x = x_\mathrm{s} + X_\mathrm{f}. \tag{15}$$

Substituting this into Eq. (3), one can collect the slow and fast flow terms and separate the original equation into the governing equation for the slow flow:

$$x_\mathrm{s}'' + 2\zeta x_\mathrm{s}' + \varepsilon \mathrm{sgn}\,(x_\mathrm{s})\,|x_\mathrm{s}|^\alpha = F\cos(\tau)\,, \tag{16}$$

where the primes denote differentiation with respect to slow time $\tau = \Omega t$ (please note that given a low-valued Ω, one holds $\Omega \ll 1$), and also the approximate governing equation for the fast flow truncated to X_f^3:

$$\begin{aligned}&\ddot{X}_\mathrm{f} + 2\zeta\dot{X}_\mathrm{f} + \varepsilon\alpha|x_\mathrm{s}|^{\alpha-1}X_\mathrm{f} + \varepsilon\alpha\,(\alpha-1)\\ &\quad \mathrm{sgn}\,(x_\mathrm{s})\,|x_\mathrm{s}|^{\alpha-2}X_\mathrm{f}^2 + \varepsilon\alpha\,(\alpha-1)\,(\alpha-2)\,|x_\mathrm{s}|^{\alpha-3}\\ &\quad X_\mathrm{f}^3 = 0,\end{aligned} \tag{17}$$

The governing equation for the slow flow (16) can be approximately solved by neglecting the damping and the inertial term. In addition, shifting the time response to have a zero displacement at the origin, Eq. (16) yields the solution for the upper outer curve of the slow flow $x_{\mathrm{s,u}}$ in the form

$$x_{\mathrm{s,u}} = \left(\frac{F}{\varepsilon}\sin(\tau)\right)^{1/\alpha}, \quad 0 \le \tau \le \pi. \tag{18}$$

The lower part $x_{\mathrm{s,l}}$ has a negative sign and is shifted along a time scale for a half of a period

$$x_{\mathrm{s,l}} = -\left(\frac{F}{\varepsilon}|\sin(\tau)|\right)^{1/\alpha}, \quad \pi \le \tau \le 2\pi. \tag{19}$$

These analytical expressions (18), (19) are plotted in Fig. 10b as red dashed lines and confirm that the slow flow stretches along these curves. Note that the slow flow and the subsequent jumps make this response resemble the relaxation oscillations that appear in a strongly damped classical van der Pol oscillator [15]. However, here, the fast flow also appears along the outer curves as reported for a bistable cubic oscillator excited at a low external angular frequency [16].

Next, the governing equation of motion for the fast flow (17) is to be solved. Regarding the existence of the nonlinearity, it contains quadratic and cubic term in X_f, i.e. it represents the Helmholtz–Duffing equation with x_s appearing in their coefficients. Such equation was derived in [17] for a bistable oscillator with cubic nonlinearity excited at low angular frequency and it

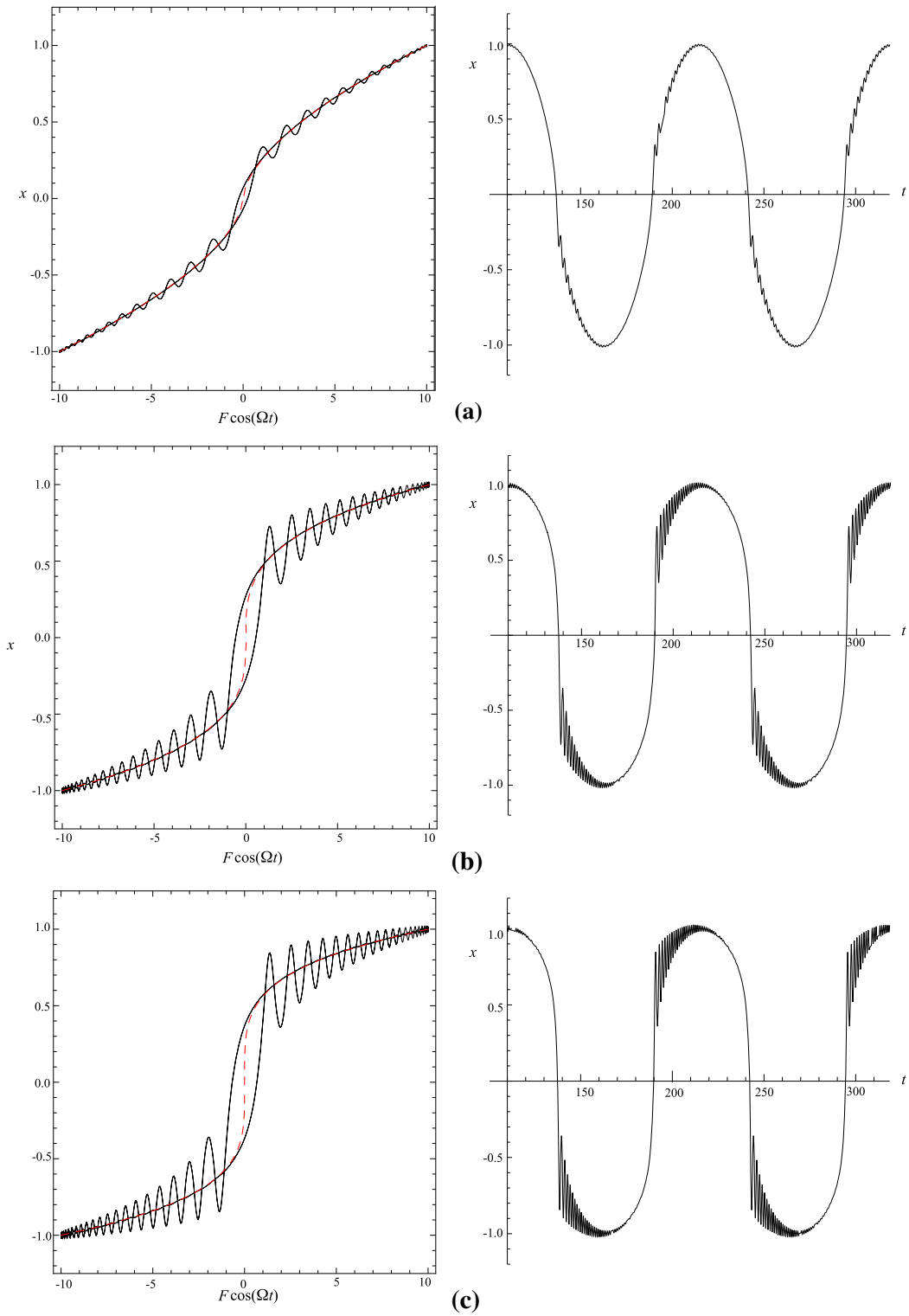

Fig. 11 Hysteretic behaviour of the response imposed on the *S-curve* (*left*) and the corresponding time responses (*right*) for: **a** $\alpha = 1.66$, **b** $\alpha = 3.1$, **c** $\alpha = 4$

involved the treatment of x_s as a constant. Although we have tried to apply the same methodology to these purely nonlinear oscillators, an acceptable accuracy could not be achieved when comparing the corresponding overall bursting oscillations with the numerical solutions of Eq. (3). A possible reason is that in bistable oscillators considered in [17], the branches of the S-curve along which the slow flow was stretched were not as curvilinear as here, which explains why it could have been taken as a constant there. Despite trying here to approximate x_s with different values (the harmonic mean, the quadratic mean, an average value obtained by integrating the slow over its periods), neither of them gave a satisfactory agreement with numerical solutions. Thus, another approach needed to be taken with $x_s(\tau)$. So, instead of treating x_s as a constant, it is taken as time-varying, i.e. the governing equation for the fast flow (17) is analysed as having slowly varying coefficients. The fast flow is taken to be governed by

$$\ddot{X}_f + 2\zeta \dot{X}_f + \varepsilon\alpha \left(\frac{F}{\varepsilon}\right)^{\frac{\alpha-1}{\alpha}} |\sin(\tau)|^{\frac{\alpha-1}{\alpha}} X_f = 0. \quad (20)$$

Note that the power of nonlinearity α of the original purely nonlinear oscillator still exists in Eq. (20). However, the quadratic and cubic terms in of X_f have been dropped from Eq. (17). To demonstrate that this is acceptable here, Eq. (20) was solved numerically, summed up with the slow flows (18), (19) and this solution is compared with the numerical solutions of Eq. (3) for a high excitation amplitude and different powers of nonlinearity: $\alpha = 1.66, 3.1, 4$. Their good matching is seen in Fig. 12a–c, which gives a reason to look for an approximate analytical solution of Eq. (20). This can be done by using the method for oscillators with slowly varying frequency [18]. Looking at Eq. (20), one can recognize this slowly varying frequency as being defined by

$$\omega(\tau) = \sqrt{\varepsilon\alpha \left(\frac{F}{\varepsilon}\right)^{\frac{\alpha-1}{\alpha}} |\sin(\tau)|^{\frac{\alpha-1}{\alpha}}}. \quad (21)$$

In addition, as 2ζ has a small value, this damping term can be treated as a perturbation, while given a small value of Ω, it is treated as a small parameter.

The solution is assumed as

$$X_f = a(t)\cos[\psi(t)], \quad (22)$$

$$\dot{X}_f = a(t)\,\omega(\tau)\sin[\psi(t)], \quad (23)$$

and the first-order differential equations for a and ψ are given by:

$$\frac{da}{dt} = -\frac{\Omega a}{2\omega(\tau)}\frac{d\omega}{d\tau} - \frac{\zeta}{\pi\omega(\tau)} \times \int_0^{2\pi} a\omega(\tau)\sin^2(\psi)\,d\psi, \quad (24)$$

$$\frac{d\psi}{dt} = \omega(\tau) - \frac{\zeta}{\pi a\omega(\tau)} \times \int_0^{2\pi} a\omega(\tau)\sin(\psi)\cos(\psi)\,d\psi. \quad (25)$$

Integrating Eq. (24), the amplitude $a(t)$ is obtained in the form

$$a(t) = \mp \sqrt{\frac{1}{\sqrt{\varepsilon\alpha\left(\frac{F}{\varepsilon}\right)^{\frac{\alpha-1}{\alpha}} |\sin(\Omega t)|^{\frac{\alpha-1}{\alpha}}} + \frac{1}{a_0^2}}}\, e^{-\zeta t}, \quad (26)$$

where a_0 is the initial amplitude. Note that the minus sign is used for the upper fast flow and the plus sign for the lower flow.

Assuming $\psi(0) = 0$, Eq. (25) is solved to obtain $\psi(t)$ in the form

$$\psi(t) = \frac{1}{\Omega}\sqrt{\varepsilon\alpha\left(\frac{F}{\varepsilon}\right)^{\frac{\alpha-1}{\alpha}}}\left(\frac{\sqrt{\pi}}{2}\frac{\Gamma\left(\frac{3}{4}-\frac{1}{4\alpha}\right)}{\Gamma\left(\frac{5}{4}-\frac{1}{4\alpha}\right)} - {}_2F_1\left[\frac{1}{2}, \frac{\alpha+1}{4\alpha}, \frac{3}{2}, \cos^2(\Omega t)\right]\cos(\Omega t)\right), \quad (27)$$

where ${}_2F_1$ stands for a hypergeometric function. The approximate solution for the fast flow given by Eqs. (22)–(27) is summed up with the slow flows (18), (19), and this solution is plotted as a magenta dotted line and compared with the numerical solutions of Eq. (3), plotted as a green solid line. The comparisons carried out for different powers of nonlinearity α are presented in Fig. 13a–c, and a very good agreement between the numerical and approximate analytical solution is seen. Note that the same parameters are used as in Fig. 12a–c. The initial amplitude a_0 is obtained numerically as the displacement from which there is a jump from the lower to the upper branch for the upper flow, and vice versa for the lower flow. It would be valuable to direct future research towards obtaining these jump amplitudes as well as the hysteresis shape analytically.

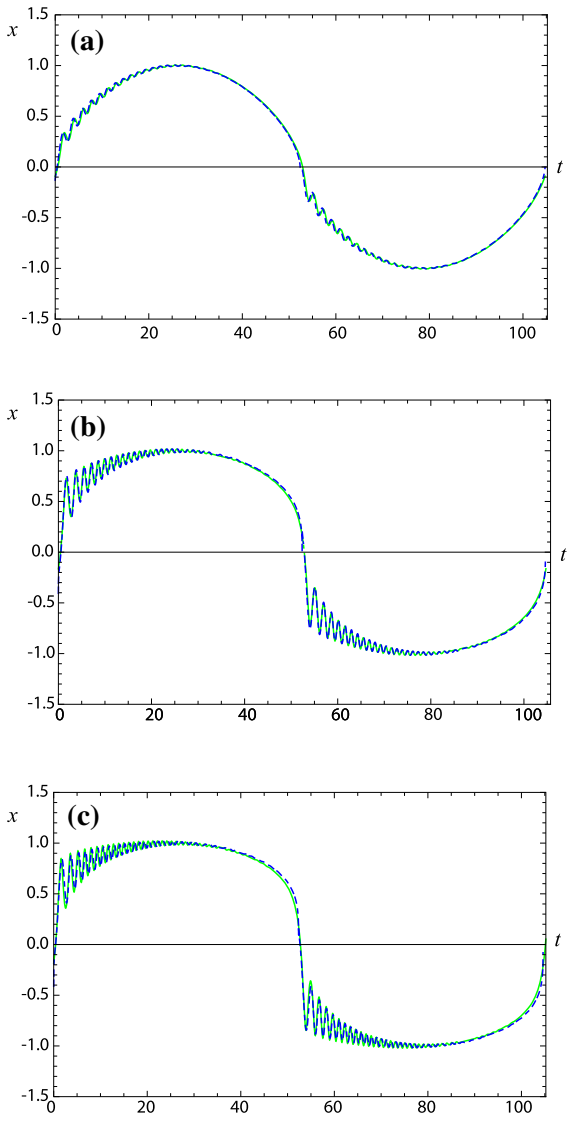

Fig. 12 Comparison of the numerical solution of Eq. (3) (*green solid line*) and the approximate solution (*blue dashed line*) obtained by summing up a numerical solution of the governing equation for the fast flow (20) with the slow flow approximation (18), (19) for: **a** $\alpha = 1.66$, **b** $\alpha = 3.1$, **c** $\alpha = 4$. (Color figure online)

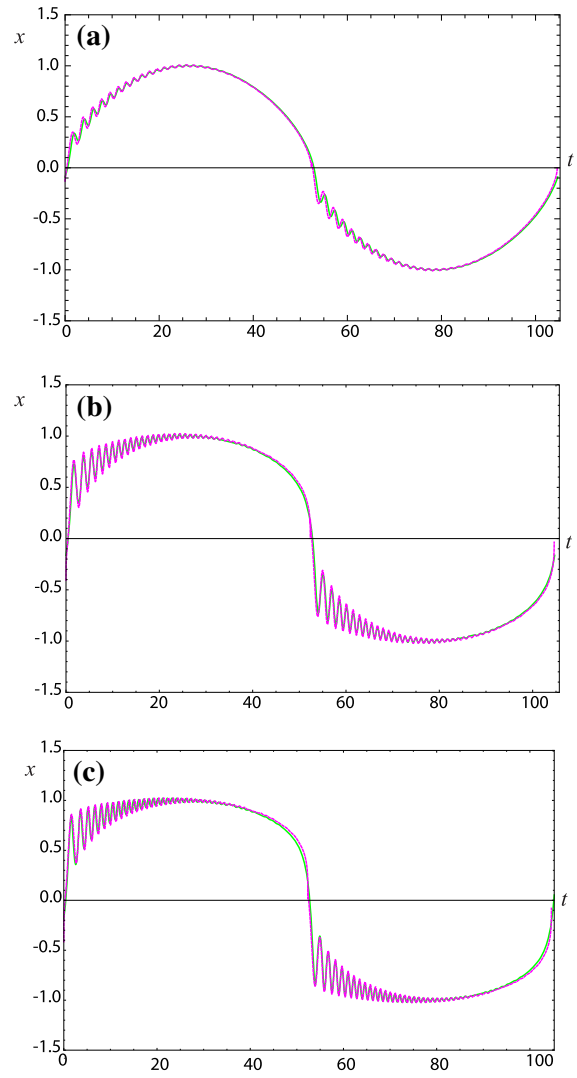

Fig. 13 Comparison of the numerical solution of Eq. (3) (*green solid line*) and the approximate solution (*green dotted line*) obtained by summing up an approximate analytical solution for the fast flow (22)–(27) with the slow flow approximation (18), (19) for: **a** $\alpha = 1.66$, **b** $\alpha = 3.1$, **c** $\alpha = 4$. (Color figure online)

4 Conclusions

This study has been concerned with a forced response of purely nonlinear oscillators with the focus on their response at different frequencies for various powers of nonlinearity.

In the first part of the study, several numerical computations have been done in order to capture the overall attractors scenario. In addition to the main attractors that have been identified also by previously published analytical techniques, many other secondary attractors have been found, including very minor ones. While likely being not directly visible in practical applications, since they exists in a very narrow range of the varying parameter and since they have a very small basin of attractions, they are indeed important as they affect the basins of attraction of the major attractors, commonly augmenting their fractality and, thus, reduc-

ing their robustness and safety. A maximum of nine coexisting attractors, symmetric and non-symmetric and of different period, have been found, showing how the multistability is a peculiarity of the considered mechanical system. The overall attractor scenario has been summarized by means of bifurcation diagrams for different powers of nonlinearity. Two different cases, one with low excitation amplitude and the other with high excitation amplitude, have been considered, and it has been shown that the overall qualitative behaviour does not change by increasing the excitation amplitude. Representative basins of attraction have been reported, and their fractality has been highlighted. An approximate analytical solution of the principal oscillation has been obtained by the Galerking method. The same solution already existing in the literature has been re-obtained herein with a different technique, showing the robustness of this analytical approximation.

In the second part of the study, an insight has been provided into the dynamic behaviour when the excitation frequency is decreased gradually until low values. It has been show how this response looks like when superimposed on the S-curve, defined by the restoring force and the excitation. Numerical results have also demonstrated that for the low-valued excitation angular frequency, the response exhibits a hysteretic behaviour, which involves bursting oscillations: it slowly moves along the lower branch of the S-curve, then jumps onto the upper branch; subsequently, there are damped fast oscillations around this upper branch; then, there is a jump from the upper to lower branch and fast damped oscillations around it appear, continuing slowly around the lower branch; afterwards, the response repeats periodically. Approximate analytical expressions for the slow and fast flow as well as for the overall bursting response have been obtained for the first time for a general class of purely nonlinear oscillators. Their good matching with numerical solutions of the corresponding governing equations has been demonstrated.

Acknowledgements The involvement of IK was financially supported by the Ministry of Science, Republic of Serbia (Project No. ON174028). The work of SL was financially supported by the SUNBEAM project (application number SUNB1400998) and was partially developed during his stay at the University of Novi Sad. The warm hospitality is gratefully acknowledged.

References

1. Kovacic, I., Brennan, M.J., Waters, T.P.: A study of a nonlinear vibration isolator with quasi-zero stiffness characteristic. J. Sound Vib. **315**, 700–711 (2008)
2. Alabudzev, P., Gritchin, A., Kim, L., Migirenko, G., Chon, V., Stepanov, P.: Vibration Protecting and Measuring Systems with Quasi-Zero Stiffness. Hemisphere Publishing, New York (1989)
3. Rivin, E.: Stiffness and Damping in Mechanical Design. Marcel Dekker Inc., New York (1999)
4. Rakaric, Z., Kovacic, I.: Approximations for motion of the oscillators with a non-negative real-power restoring force. J. Sound Vib. **330**, 321–336 (2011)
5. Mickens, R.E.: Truly Nonlinear Oscillations: Harmonic Balance, Parametric Expansions, Iteration, and Averaging Methods. World Scientific, Singapore (2010)
6. Hayashi, C.: Nonlinear Oscillations in Physical Systems. McGraw-Hill, New York (1964)
7. Burton, T.D.: A perturbation method for certain non-linear oscillators. Int. J. Non-Linear Mech. **19**, 397–407 (1984)
8. Burton, T.D., Rahman, Z.: On the multiple-scale analysis of strongly non-linear forced oscillators. Int. J. Non-Linear Mech. **21**, 135–146 (1986)
9. Kovacic, I.: Forced vibrations of oscillators with a purely nonlinear power-form restoring force. J. Sound Vib. **330**, 4313–4327 (2011)
10. Kovacic, I.: The method of multiple scales for forced oscillators with some real-power nonlinearities in the stiffness and damping force. Chaos Solitons Fractals **44**, 891–901 (2011)
11. Rakaric, Z., Kovacic, I.: An elliptic averaging method for harmonically excited oscillators with a purely non-linear non-negative real-power restoring force. Commun. Nonlinear Sci. Numer. Simul. **18**, 1888–1901 (2013)
12. http://mathworld.wolfram.com/GammaFunction.html. Accessed 5 July 2017
13. Rega, G., Lenci, S.: A global dynamics perspective for system safety from macro-to nanomechanics: analysis, control, and design engineering. Appl. Mech. Rev. **67**, 050802 (2015)
14. Rega, G., Lenci, S.: Identifying, evaluating, and controlling dynamical integrity measures in non-linear mechanical oscillators. Nonlinear Anal Theory Methods Appl. **63**, 902–914 (2005)
15. Rand, R.H.: Lecture Notes on Nonlinear Vibrations (version 53). http://dspace.library.cornell.edu/handle/1813/28989
16. Han, X.J., Bi, Q.S.: Bursting oscillations in Duffing equation with slowly changing external forcing. Commun. Nonlinear Sci. Numer. Simul. **16**, 4146–4152 (2011)
17. Kovacic, I., Cartmell, M.P., Zukovic, M.: Mixed-mode dynamics of bistable oscillators with low-frequency excitation: behavioural mapping, approximations for motion and links with van der Pol oscillators. Proc. R. Soc. A **471**, 20150638 (2015)
18. Bogoliubov, N.N., Mitropolsky, Y.A.: Asymptotic Methods in the Theory of Non-Linear Oscillations. Nauka, Moscow (1974). **(In Russian)**